X-Ray analysis and excited state dynamics in a new class of lanthanide mixed chelates of the type $LnPh\beta_3 \cdot Phen$ (Ln = Sm, Eu, Gd, Tb)

Grażyna Oczko,[a] Janina Legendziewicz,*[a] Victor Trush[b] and Vladimir Amirkhanov[b]

[a] *Faculty of Chemistry, University of Wrocaw, F. Joliot-Curie 14, 50-383, Wrocaw, Poland. E-mail: jl@wchuwr.chem.uni.wroc.pl; Fax: +48 71 3282348; Tel: +48 71 3757300*
[b] *Institute of Chemistry, Kiev State University, Vladimirskaya 64, 2520033, Kiev, Ukraine*

Received (in Montpellier, France) 8th November 2002, Accepted 23rd January 2003
First published as an Advance Article on the web 1st May 2003

A new type of lanthanide complex with a derivative of β-diketone and phenanthroline, $LnPh\beta_3$·Phen [where $Ph\beta = CCl_3–C(O)–N–P(O)–(OCH_3)_2$; Phen = 1,10-phenanthroline, Ln = Sm, Eu, Gd, Tb] was synthesised. The X-ray diffraction analysis of the Sm(III) complex shows that it is in the monoclinic system and $P2_1/c$ space group. There are two different Sm^{3+} ions with insignificant differences between the Sm–O, –N distances (0.005 Å) and a CN = 8. Absorption, emission and emission excitation spectra at 293, 77 and 4.2 K were used to characterise the title compounds in the solid state and in solution. The luminescence spectra at 77 K for the Eu analogue are complex and two components in the $^5D_0 \rightarrow {}^7F_0$ transition show that Eu^{3+} ions reside in two symmetry sites. The spectroscopic results correspond well to the crystal structure of the $SmPh\beta_3$·Phen compound and confirm that the Sm^{3+}, Eu^{3+} and Tb^{3+} monocrystals are isostructural. Efficient energy transfer sensitises the interion emission from $^5D_4$ or $^5D_0$ levels of Tb(III) and Eu(III) after ligand band excitation. Based on the splitting of the levels observed at 4.2 K in the single crystal spectra of Tb and Eu, as well as the absorption, phosphorescence and excitation spectra, energy level diagrams are proposed. The mechanism of energy transfer and excited state dynamics are discussed. Strong vibronic coupling was observed mainly in the $^7F_0 \rightarrow {}^5D_2$ electronic transition. The IR spectra were used to analyse the vibronic components. Analysis of the emission spectra of a Eu^{3+}-doped silica sol-gel sample was made and compared to those for the title monocrystals. The total spectral characteristics of the materials permits an evaluation of their potential applicability.

Introduction

Molecules capable of carrying out efficient light conversion may find a number of applications, mainly in optical devices, luminescence sensors, fluorescent lighting and electroluminescent devices.[1–5] Recently we have reported results of optical studies for the series of lanthanide chelates of the type $Ln\beta_3L$, L, which can be used in electroluminescent devices.[2–4]

Now we present a new type of lanthanide complex with dimethyl trichloroacetylamidophosphate (denoted as Phβ) and 1,10-phenanthroline (a Lewis base ligand) as ligands. Since this class of compounds has the perspective of applications in optical devices and also as anticancer agents, they are of interest for our studies.

1,10-Phenanthroline (Phen) has always attracted interest because it has rigid structure imposed by the central ring, such that the two nitrogen atoms are always in juxtaposition, whereas, for example in 2,2′-dipyridyl systems, free rotation about the linking bond allows the two nitrogens to separate. This entropic advantage for Phen means that formation of complexes with metal ions is faster.[6] Another important property of Phen is its triplet state photosensitising ability, especially in complexes with lanthanides such as europium and terbium.[2,7] The knowledge of the photophysics of this kind of lanthanide chelate is not currently at a satisfactory level.

With the aim of shedding light on this area an effort was made to synthesise monocrystals of a new class of lanthanide compounds of the $LnPh\beta_3$·Phen type [where $Ph\beta = CCl_3–C(O)–N–P(O)–(OCH_3)_2$; Phen = 1,10-phenanthroline, Ln = Sm, Eu, Gd, Tb]. Undoubtedly, the important spectral characteristics of these materials can be controlled by the donor-acceptor properties and is responsible for the location of the energy levels, the efficiency of energy-transfer, electron-phonon coupling and finally the luminescence quantum yield. Correlation of photophysical properties and the crystal

Table 1 The crystal data and structure refinement for $SmPh\beta_3$·1,10-Phen

Empirical formula	$C_{24}H_{26}Cl_9N_5O_{12}P_3Sm$
Formula weight	1138.81
T/K	220(2)
λ/Å	0.71073
Crystal system	Monoclinic
Space group	$P2_1/c$
a/Å	19.480(2)
b/Å	21.875(2)
c/Å	21.415(3)
β/°	109.459(8)
U/Å^3	8604(2)
Z	8
μ/mm^{-1}	2.093
Reflections collected	45 528
Independent reflections	17 509
R_{int}	0.0595
$R1$ [$I > 2\sigma(I)$]	0.0611
$wR2$ [$I > 2\sigma(I)$]	0.0979
$R1$ (all data)	0.1317,
$wR2$ (all data)	0.1241

 DOI: 10.1039/b211044j

Table 2 Selected bond lengths (Å) and angles (°) for $SmPh\beta_3$·1,10-Phen

Sm(1)–O(1)	2.342(5)	Sm(2)–O(21)	2.343(5)
Sm(1)–O(9)	2.358(5)	Sm(2)–O(17)	2.351(5)
Sm(1)–O(5)	2.370(5)	Sm(2)–O(13)	2.353(5)
Sm(1)–O(6)	2.418(5)	Sm(2)–O(22)	2.407(6)
Sm(1)–O(10)	2.420(5)	Sm(2)–O(14)	2.436(5)
Sm(1)–O(2)	2.426(5)	Sm(2)–O(18)	2.452(5)
Sm(1)–N(10)	2.573(5)	Sm(2)–N(8)	2.582(6)
Sm(1)–N(9)	2.592(6)	Sm(2)–N(7)	2.606(6)
Sm(1)–Sm(2)	11.768		
O(1)–Sm(1)–O(9)	108.4(2)	O(6)–Sm(1)–N(10)	108.8(2)
O(1)–Sm(1)–O(5)	146.2(2)	O(10)–Sm(1)–N(10)	139.6(2)
O(9)–Sm(1)–O(5)	82.1(2)	O(2)–Sm(1)–N(10)	76.5(2)
O(1)–Sm(1)–O(6)	138.8(2)	C(21)–O(6)–Sm(1)	132.9(5)
O(9)–Sm(1)–O(6)	85.9(2)	P(3)–O(9)–Sm(1)	135.9(3)
O(5)–Sm(1)–O(6)	72.3(2)	C(31)–O(10)–Sm(1)	139.0(5)
O(1)–Sm(1)–O(10)	73.0(2)	P(4)–O(13)–Sm(2)	134.7(3)
O(9)–Sm(1)–O(10)	72.1(2)	C(41)–O(14)–Sm(2)	134.2(5)
O(5)–Sm(1)–O(10)	139.7(2)	P(5)–O(17)–Sm(2)	135.5(3)
O(6)–Sm(1)–O(10)	75.4(2)	C(51)–O(18)–Sm(2)	137.3(5)
O(1)–Sm(1)–O(2)	72.5(2)	P(6)–O(21)–Sm(2)	132.3(3)
O(9)–Sm(1)–O(2)	76.0(2)	C(61)–O(22)–Sm(2)	138.1(5)
O(5)–Sm(1)–O(2)	79.5(2)	C(1)–N(1)–P(1)	122.3(6)
O(6)–Sm(1)–O(2)	148.3(2)	C(21)–N(2)–P(2)	122.1(6)
O(10)–Sm(1)–O(2)	121.5(2)	C(31)–N(3)–P(3)	122.3(5)
O(1)–Sm(1)–N(10)	80.4(2)	C(41)–N(4)–P(4)	122.3(6)
O(9)–Sm(1)–N(10)	146.8(2)	C(51)–N(5)–P(5)	122.8(5)
O(5)–Sm(1)–N(10)	74.8(2)	C(61)–N(6)–P(6)	121.1(6)

structure of the title compounds and of other lanthanide chelates will be made.

Experimental

Synthesis of $LnPh\beta_3 \cdot Phen$ chelates (Ln = Sm, Eu, Gd, Tb) and doped sol-gel samples

The synthesis was performed according to the reaction:[8,9]

$$Ln(X)_3 \cdot 6H_2O + 3Na\{Ph\beta\} + Phen + 6HC(OEt)_3 \rightarrow \{LnPh\beta_3 \cdot Phen\} + 3NaX + 6HC(O)OEt + 12EtOH$$

with X = Cl^- or NO_3^- and {Phβ} = dimethyl trichloroacetylamidophosphate anion.

$LnCl_3 \cdot 6H_2O$, $Ln(NO_3)_3 \cdot 6H_2O$ and 1,10-phenanthroline monohydrate (Phen) were of commercial grade used without further purification. The procedures for the synthesis of H(Phβ) and its sodium salt Na(Phβ) were described previously.[10,11] $HC(OEt)_3$ (1 ml, 6 mmol) was added to a boiling solution of 1 mmol of lanthanide(III) nitrate (chloride) in 10 ml of dry acetone. A solution of 0.8773 g (3 mmol) of Na(Phβ) in 10 ml of dry acetone and then one of 0.1762 g (1 mmol) of dry Phen in 5 ml of acetone were added. The $NaNO_3$ (NaCl) precipitate was filtered off. The solution was evaporated under vacuum to a volume of about 2 ml. *Ca.* 15 ml of 2-propanol was added to the previous solution, which was then dried in a vacuum desiccator over $CaCl_2$. After 1–2 days monocrystals of the complex precipitated. The yield of the target complex was about 90%. The complexes are stable in air, soluble in polar organic solvents and almost insoluble in water. The lanthanide ion content in the final complexes was determined by complexometric EDTA titration with xylenol orange as indicator.

Ln^{3+} (Eu^{3+}, Sm^{3+})-doped silica sol-gel samples were prepared by the acid-catalysed hydrolysis of tetraethylorthosilicate (TEOS) with deionized water and polycondensation. An acetonitrile solution of the $LnPh\beta_3$·Phen complex (1 mmol) was added. The TEOS:water:acetonitrile molar ratio was 1:0.5:7. This solution was stirred for 2 h in a small polypropylene vial at room temperature. After homogenisation, the sols were stored for gelation in the same vial, covered by a small glass, at room temperature for 2 days. After 4 weeks transparent monolithic dried solid samples of cylindrical shape were obtained.

An ICP-AES spectrometer was used to determine the lanthanide ion concentration in the sol-gel samples.

Spectroscopic measurements

The high resolution absorption spectra of $LnPh\beta_3$·Phen (Ln = Sm, Eu) single crystals were obtained at 293 and at 4.2 K using a Cary–Varian 500 UV-Vis-near-IR spectrophotometer equipped with an Oxford CF 1204 continuous flow

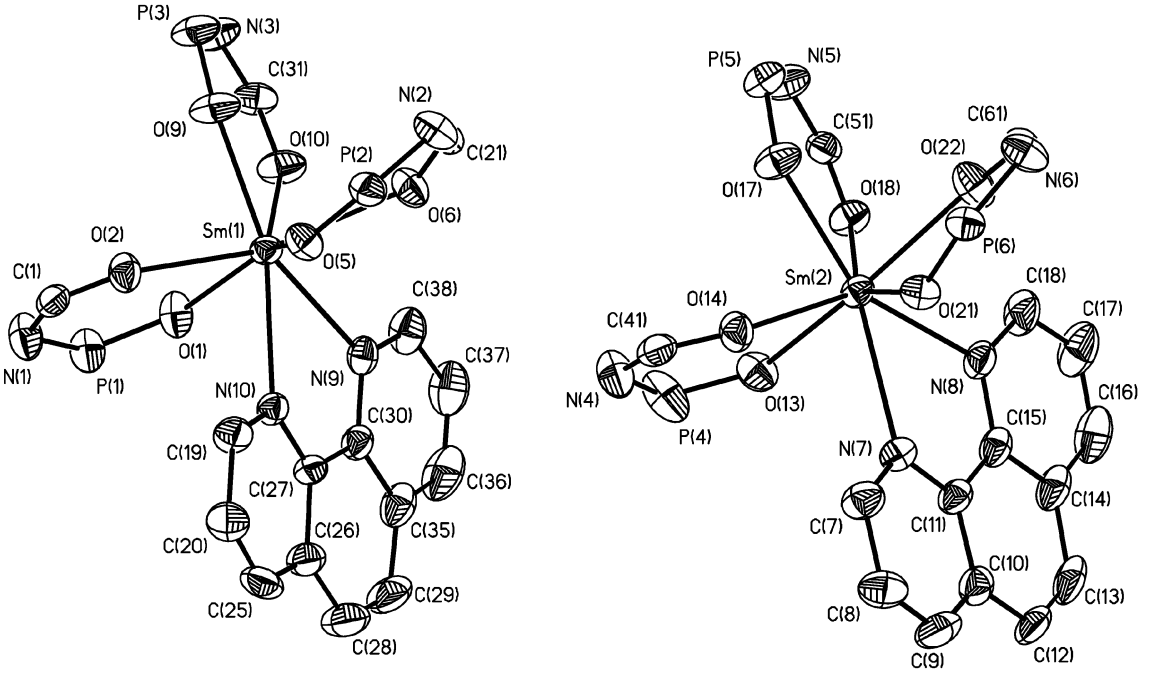

Fig. 1 Structure of the $SmPh\beta_3$·1,10-Phen complex (on the left for Sm_1; on the right for Sm_2). The hydrogen atoms, CCl_3^- and methoxy groups are omitted for clarity.

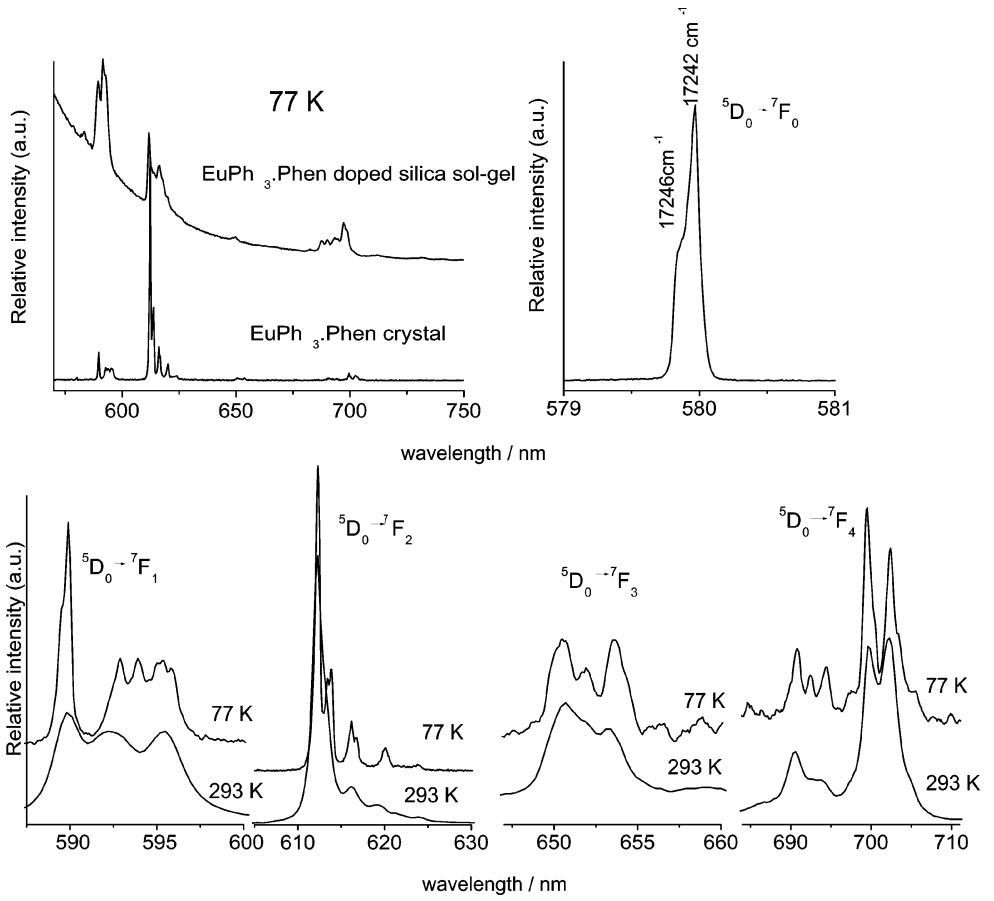

Fig. 2 Fluorescence spectra of the EuPhβ$_3$·1,10-Phen crystal and the spectra of co-doped silica sol-gel at 293 and 77 K; $\lambda_{ex.} = 350.5$ nm.

helium cryostat, in the 350–1700 nm spectral range. The areas of the absorption bands were determined numerically by the graphical integration method and are expressed in terms of the oscillator strengths, using the programme described in ref. 12:

$$P = 4.33 \times 10^{-9} \int_{\sigma_1}^{\sigma_2} \varepsilon(\sigma)\mathrm{d}\sigma \qquad (1)$$

where $\varepsilon(\sigma)$ is the molar extinction coefficient of the band at the wave number σ (in cm^{-1}). The experimental oscillator strength values were used for calculation of the Judd–Ofelt parameters τ_λ (in cm)[13,14] according to the following equation in the form given by Carnall:[15]

$$P = \sum_{\lambda=2,4,6} \tau_\lambda \sigma \left(\mathrm{f}^N \Psi_J \parallel U^{(\lambda)} \parallel \mathrm{f}^N \Psi'_{J'} \right)^2 \Big/ (2J+1) \qquad (2)$$

where $(\mathrm{f}^N\Psi_J\|\mathbf{U}^{(\lambda)}\|\mathrm{f}^N\Psi'_{J'})$ are the reduced matrix elements of the unit tensor operator $\mathbf{U}^{(\lambda)}$, calculated by Carnall *et al.*[16] In the intermediate coupling scheme $\mathrm{f}^N\Psi_J$ and $\mathrm{f}^N\Psi'_{J'}$ are the initial and final states of the electronic transition and J is the total quantum number.

The emission and emission excitation spectra of LnPhβ$_3$·Phen (Ln = Eu, Tb) were recorded at 293 and 77 K using a SLM Aminco SPF 500 spectrofluorometer. Phosphorescence of the gadolinium analogue was detected at 77 and 4.2 K.

The IR spectra, in KBr pellets, were recorded in the range of 50–4000 cm^{-1} using a Bruker IFS 113v spectrophotometer.

Crystallography

Crystals of dimensions $0.40 \times 0.35 \times 0.30$ mm^3 were used for the X-ray diffraction study. Crystallographic measurements for SmPhβ$_3$·Phen were made at 220 K using a SMART CCD area detector diffractometer (Siemens). Semi-empirical absorption corrections using the SADABS program were applied. Table 1 lists the cell parameters and details of the data acquisition and structure refinement. The structures were solved by direct methods and subsequent Fourier difference techniques and refined using the programs SHELXS-86 and SHELXL-93.[17,18] All non-hydrogen atoms were refined anisotropically; the hydrogen atoms were included in the calculations as fixed contributions with their isotropic U values set invariant at 0.08 Å^2. Refinements were terminated with all

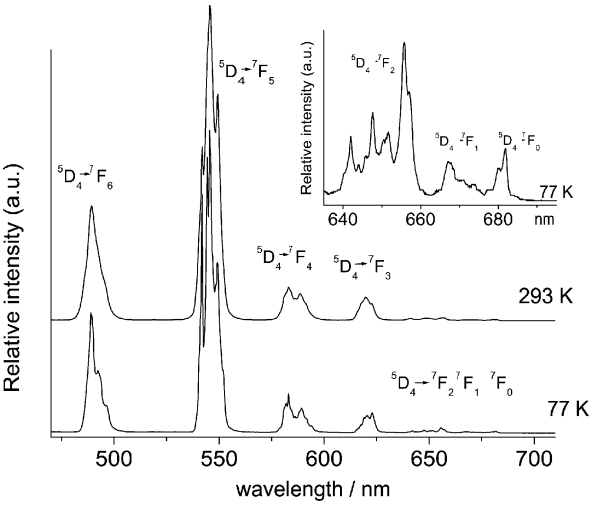

Fig. 3 Fluorescence spectra of the TbPhβ$_3$·1,10-Phen crystal at 293 and 77 K; $\lambda_{ex.} = 350.5$ nm.

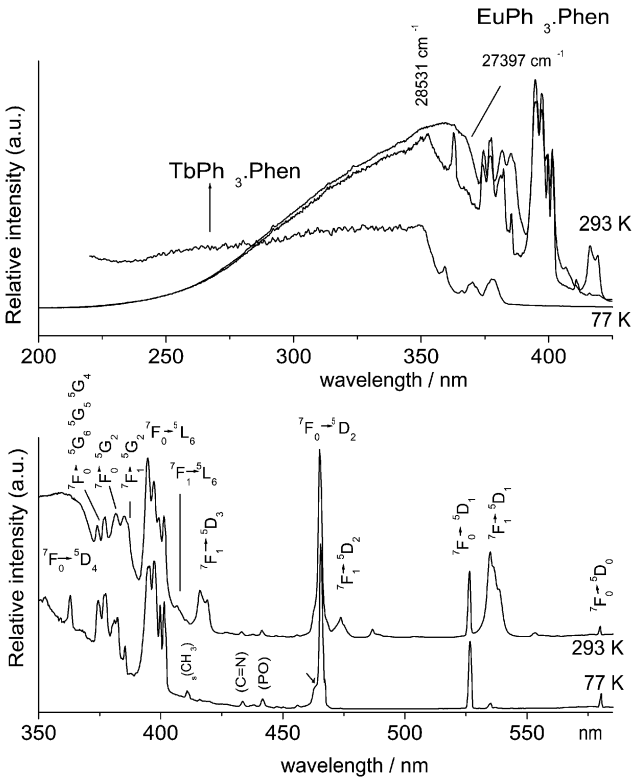

Fig. 4 Fluorescence excitation spectra of the $LnPh\beta_3$·1,10-Phen (Ln = Eu, Tb) crystals at 293 and 77 K; $\lambda_{mon.}$ = 612.2, 545.7 nm.

non-hydrogen parameter shifts $< 0.20\sigma$; the weighting scheme was $w^{-1} = \sigma^2(F^2) + (aP)^2 + bP$, where $3P = (2F_c^2 + F_o^2)$ and a and b are constants adjusted by the program. Convergence was obtained at the R values given in Table 1. Selected interatomic distances and angles are listed in Table 2. CCDC reference number 201037. See http://www.rsc.org/suppdata/nj/b2/b211044j/ for crystallographic files in CIF or other electronic format.

Results and discussion

X-Ray structures

The lanthanide mixed chelates of the type $LnPh\beta_3$·Phen [where Ln = Sm, Eu, Tb; Phβ = CCl_3–C(O)–N–P(O)–$(OCH_3)_2$; Phen = 1,10-phenanthroline] create an isotypic series. $SmPh\beta_3$·Phen crystallises in the monoclinic space group $P2_1/c$, $Z = 8$ with unit cell parameters $a = 19.480(2)$, $b = 21.875(2)$, $c = 21.415(3)$ Å, $\beta = 109.459(8)°$ (see Table 1). The geometries of the Sm(III) ion environments in $SmPh\beta_3$·Phen crystal are shown in Fig. 1. The X-ray diffraction studies detect two different Sm^{3+} sites in the $SmPh\beta_3$·Phen monocrystal, which is not very common in this type of chelates.[4,7,19,20] The Sm^{3+} ions adopt an 8-coordinate geometry with 6 oxygen atoms from the Phβ ligand and two nitrogen atoms from Phen molecules. The mean values of the Sm_1–L and Sm_2–L (L = ligand) bond lengths are insignificantly different: Sm(1)–L 2.486 Å and Sm(2)–L 2.491 Å (see Table 2), but larger differences were observed for the angles between the Phen plane and the Phβ planes in both samarium ion sites (153.6°, 118.9°, 73.5°; 153.1°, 109.9°, 86.5°). These factors are responsible for the creation of the dissimilar environments about the Sm^{3+} ions in the crystal structure and finally lead to subtle differences in the symmetry of the metal ion sites, which can be reflected in the spectroscopic results.

Spectroscopic results for the Eu(III), Tb(III) and Gd(III) systems

Among the trivalent lanthanide ions, Eu(III) is especially useful as an optical probe of ligand or crystal field perturbations on 4f electron energy levels and radiative transition properties. The ground state multiplet $^7F_0$ is non-degenerate and the principal emitting state, in most cases $^5D_0$, is also non-degenerate. Therefore, the initial states in absorption, $^7F_0 \rightarrow {}^5D_J$, and in emission, $^5D_0 \rightarrow {}^7F_J$, remain uncomplicated even in low-symmetry ligand environments. Furthermore, in emission each $^5D_0 \rightarrow {}^7F_J$ transition has origins appearing in well-separated spectral regions. Although additional transitions from $^7F_1$ and $^7F_2$ states populated at room temperature lead to a complex structure of the absorption and emission excitation spectra and sometimes f-f transitions are obscured by low-lying ligand-to-Eu(III) charge-transfer transitions, even in these cases

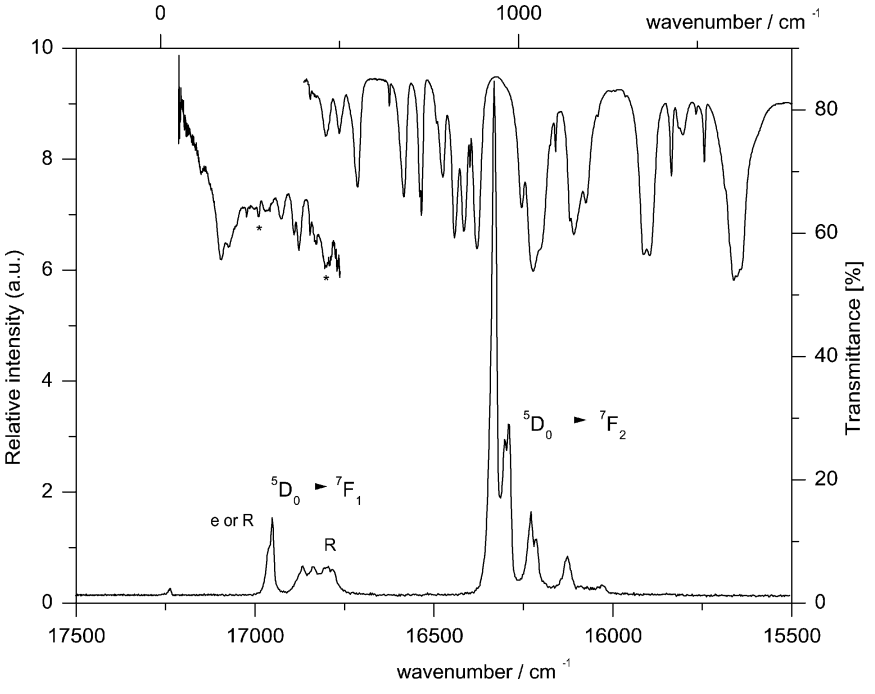

Fig. 5 Superposition of IR and fluorescence spectra of the $EuPh\beta_3$·1,10-Phen crystal.

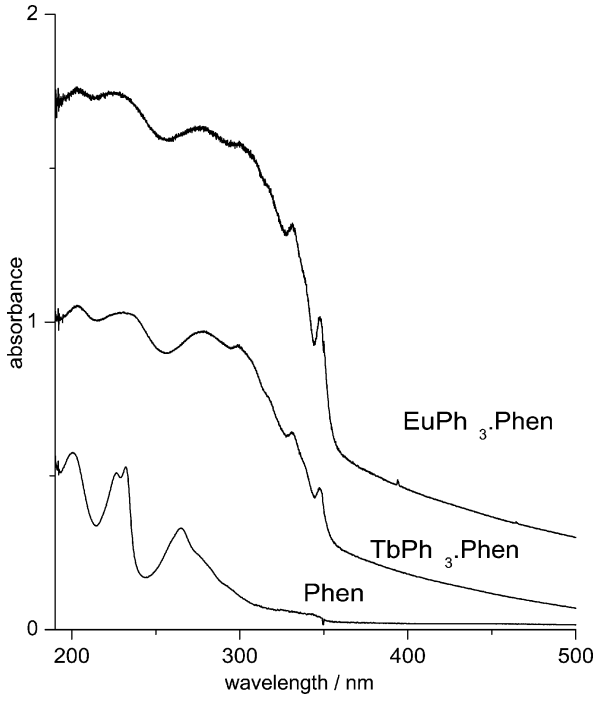

Fig. 6 Absorption spectra of the LnPhβ$_3$·1,10-Phen crystals in paraffin oil at 293 K (Ln = Eu, Tb).

the spectra can be easily analysed. This is explained by the fact that among all the expected f-f transitions only $^5D_0 \rightarrow {}^7F_1$ satisfies $\Delta J = 0, \pm 1$ (excluding $J = J' = 0$), the intermediate coupling selection rule for magnetic dipole transition intensity, and is only weakly dependent on the crystal field effects. On the other hand, considering the odd-parity components of the crystal field potential, only $^5D_0 \rightarrow {}^7F_{2,\ 4,\ 6}$ transitions are electric-dipole allowed (in the absence of J level mixing)[21] and strongly dependent on the odd-parity components of the crystal field. The $^5D_0 \rightarrow {}^7F_{0,\ 1,\ 3,\ 5}$ transitions cannot acquire electric dipole intensity, and their magnetic dipole intensities can occur only to the first order in the even-parity crystal field components. In agreement with the above considerations, unpolarised emission spectra over the 520–720 nm spectral region show $^5D_0 \rightarrow {}^7F_{0,\ 1,\ 2,\ 3,\ 4}$ emissions and very weak, almost undetectable, $^5D_{1,\ 2} \rightarrow {}^7F_J$ emissions.

Since the red emission of Eu(III) and the green one of Tb(III) can find wide optical applications, we extended our studies to Tb(III) chelate. Furthermore, the spectroscopy of these ions together with the phosphorescence of Gd(III) chelate can help to explain the mechanism of the energy transfer processes that sensitise the interion emission, thus our spectroscopic consideration will be in the order: Eu(III), Tb(III), Gd(III) and Sm(III). The latter is a special case of good applicability of Judd–Ofelt theory of the f-f transition probability.

The fluoroscence spectra for both EuPhβ$_3$·Phen and TbPhβ$_3$·Phen at 293 and 77 K, presented in Figs. 2 and 3, are complex. All the bands that correspond to their respective transitions are composed of more components than expected for a one-site symmetry of Ln^{3+} ions. At 77 K two components of the $^5D_0 \rightarrow {}^7F_0$ transition of Eu(III) ($\Delta E = 4$ cm^{-1}) were detected, whereas 6 components for the $^5D_0 \rightarrow {}^7F_1$ band and a clear doublet structure for the $^5D_0 \rightarrow {}^7F_2$ transition point to two different Eu^{3+} sites of low symmetry in the EuPhβ$_3$·Phen crystal (see Fig. 2). Assignments of the respective f-f transitions in emission and excitation spectra of the Eu(III) chelate are given in Figs. 2 and 4.

Careful analysis of the respective components of the $^5D_0 \rightarrow {}^7F_{1,\ 2}$ transitions indicates additional splitting of the Stark components at 596 and 617 nm. Since relatively strong vibronic components were detected in the excitation spectra and in the high energy region of the $^7F_0 \rightarrow {}^5D_2$ transition, the phenomenon observed in the range of the $^5D_0 \rightarrow {}^7F_{1,\ 2}$ transitions could be the result of electron-phonon coupling. Superposition of the IR and europium emission spectra (see Fig. 5) makes an analysis of the vibronic components in the emission spectra possible; the modes δ(OPO) or ν(OLnO)*π(φ)

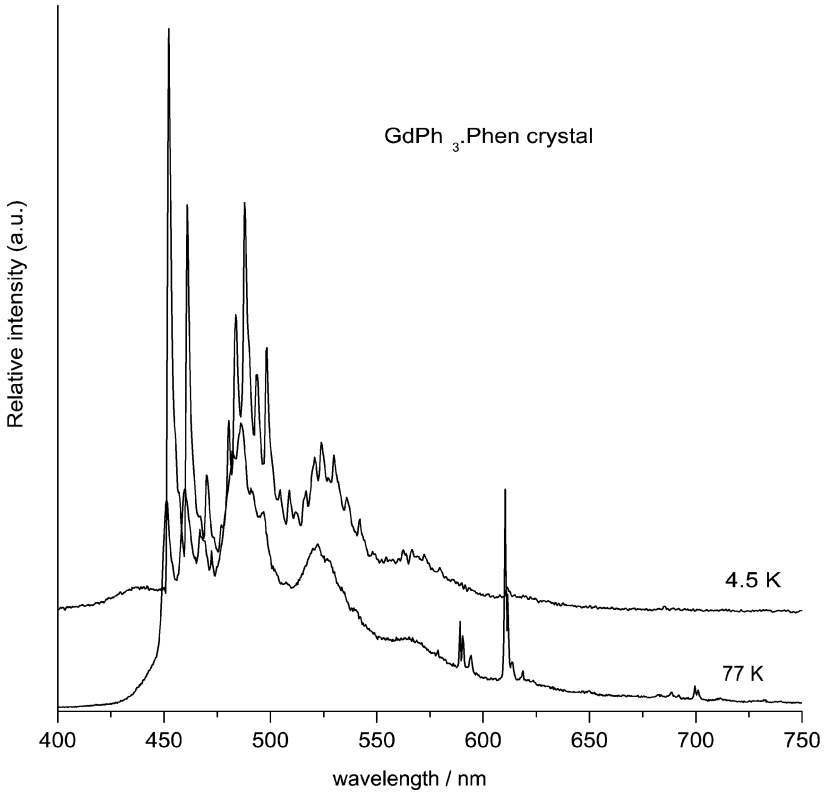

Fig. 7 Phosphorescence spectra of the GdPhβ$_3$·1,10-Phen crystal at 77 and 4.2 K.

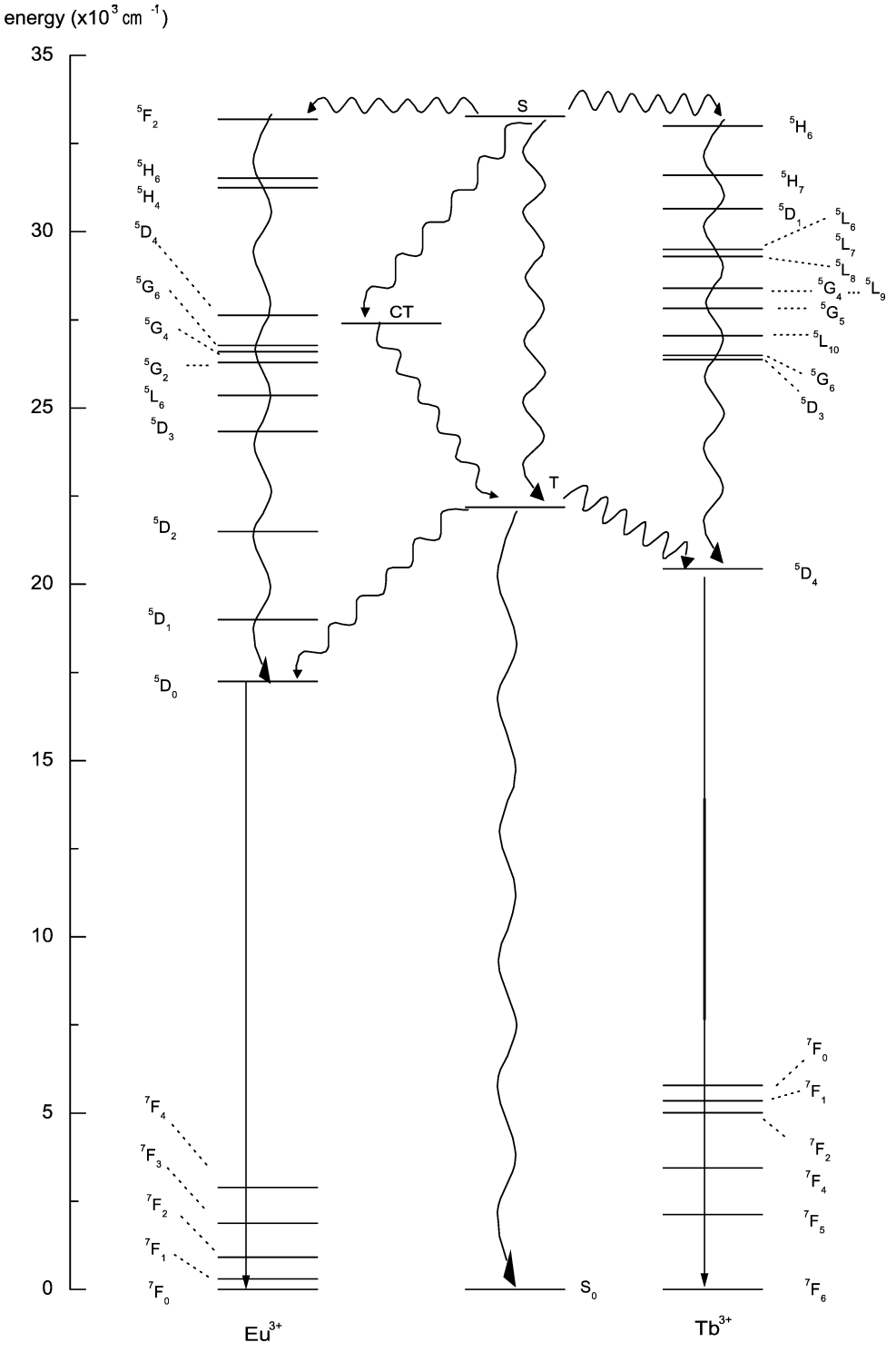

Fig. 8 Energy level diagrams for the LnPhβ$_3$·1,10-Phen (Ln = Eu, Tb) systems.

at 276 cm^{-1} and $\delta(CCl_3)$*$\delta(\phi_n)$ at 458 cm^{-1} are responsible for additional splitting as the result of resonance. Moreover, in the spectra the $^5D_0 \rightarrow {}^7F_2$ band is the strongest one and significantly more intense than the $^5D_0 \rightarrow {}^7F_1$ one, indicating relatively low symmetry of the metal centre.

Fig. 6 presents the absorption spectra of solid europium and terbium complexes. Strong absorption bands in the UV region correspond to $^1\pi$-π^*, $^3\pi^*$ transitions, mainly in the phenanthroline molecules. Comparison of the absorption spectra with the respective excitation spectra points to the role of surface quenching because, finally, stronger excitation was observed using the 350 nm excitation line, that is in the tail of the strong absorption band at 290 nm (see Figs. 4 and 6), than using other excitation lines.

Fig. 4 displays the fluorescence excitation spectra of LnPhβ$_3$·Phen (Ln = Eu, Tb). These spectra show significant differences in the location and intensities of the bands compared to those in the absorption spectra. The ligand transitions are localised at energies higher than 28 571 cm^{-1} (350 nm), which corresponds to $^1\pi\pi^*$ and $^3\pi\pi^*$ transitions of the conjugated systems of Phen and the second ligand, similar to that observed by Legendziewicz *et al.*[2,4,19,20,22] and by Bünzli *et al.*[7] In this range also the charge-transfer state in the europium chelate can be localised. Comparison of EuPhβ$_3$·Phen and TbPhβ$_3$·Phen fluorescence excitation spectra locates the charge transfer (CT) state for europium (at approximately 27 397 cm^{-1}), which is overlapped by ligand transitions. The discrepancy between absorption and excitation spectra was

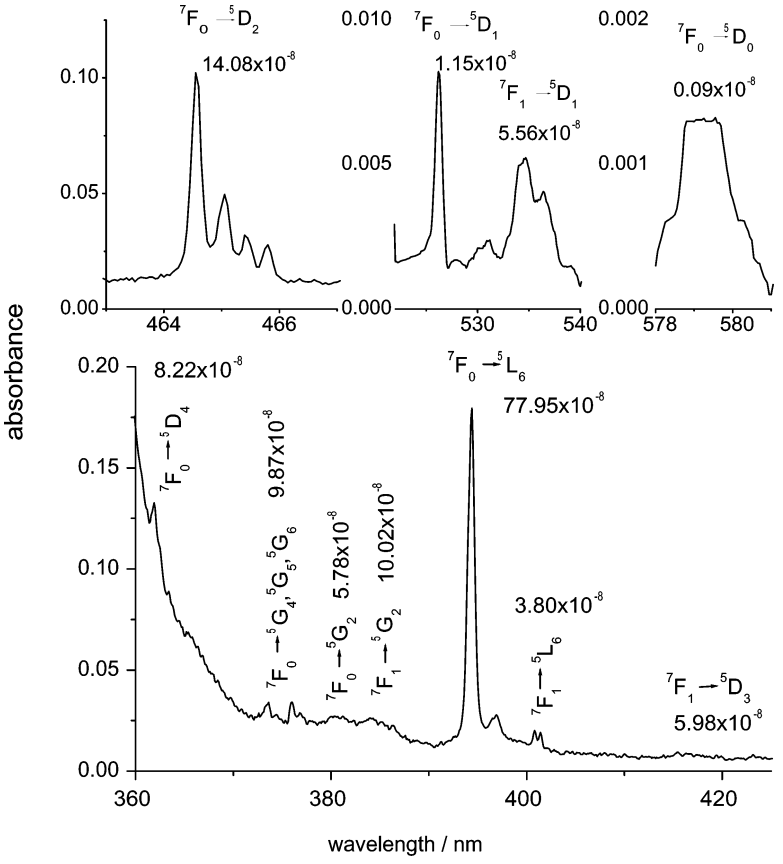

Fig. 9 Absorption spectrum of the EuPhβ$_3$·1,10-Phen crystal at 293 K and the oscillator strength values of the f-f transitions.

also observed by Blasse *et al.*[23] in lanthanide crystals and by ourselves.[24]

The emission spectra of Tb(III) compound at 293 and 77 K are presented in Fig. 3. Similar to the splitting observed in the $^5D_0 \rightarrow {}^7F_J$ transitions of Eu(III), the doublet structure is manifested in Tb(III) chelate spectra at low temperature, which suggests a similar structure of the crystals. X-Ray analysis was also used to check the isomorphism of the Tb(III) and Sm(III) chelates. Strong green emission was detected by ligand excitation (350 nm), but with a somewhat lower efficiency than in the the Eu(III) system. This is reasonable since ΔE between the ligand T state and the $^5D_4$ level is relatively large and these levels are not in resonance. Most probably this energy transfer can be phonon-assisted, because the interion emission excited by the ligand state is more efficient than that excited directly to the $^5D_4$ Tb(III) level. Since the charge-transfer state for Tb(III) cannot lie in the analysed spectral range (see Fig. 4), comparison of the Eu(III) and Tb(III) excitation spectra can help in localisation of the L–Eu CT state. Thus, it can be concluded that the CT state for Eu(III) is situated at approximately 365 nm. The room temperature spectrum of Eu(III) shows significant population of the $^7F_1$ and $^7F_2$ levels at 293 K, as was expected and observed in other lanthanide chelates.[25]

Based on the low temperature absorption, emission and emission excitation spectra, energy level diagrams are proposed for both the Eu(III) and Tb(III) chelates. The energy of the Gd(III) excited ^6P_J levels are above the ligand triplet state, thus phosphoroscence of the ligand, displayed in Fig. 7, can be easily observed. The fine vibronic structure is seen in the spectra at 4.5 K with ~1400 cm^{-1} energy replica. The energy of the ligand triplet state was determined from the above spectra to be 22 183 cm^{-1}. In this way a mechanism for the energy transfer is proposed (Fig. 8). Energy can be transferred directly from the phenanthroline singlet (S) state to high-lying europium or terbium states and through intersystem crossing (ISC) to the ligand triplet (T) state and further to the $^5D_2$ level in the Eu(III) case by multipolar interaction, since this level is almost in resonance with the ligand T state. Moreover, the CT state of Eu(III) can be involved in these processes as well and can increase the ligand T state population or can be non-radiatively deactivated. In the case of the Tb(III) chelate, the CT state in the considered energy region can be neglected and energy can be transferred directly from the ligand S state to high-lying states of Tb(III) or by ISC to the T state and then to the $^5D_4$ emitting level.

Absorption spectra of the Eu(III) chelate in the 350–590 nm are shown in Fig. 9. The assignments of the f-f transitions together with their oscillator strength values are also indicated on Fig. 9. The oscillator strength of the hypersensitive transition $^7F_0 \rightarrow {}^5D_2$, which is markedly affected by the metal environment, is relatively high, which confirms the rather low symmetry of the metal centre.

Sm(III) spectroscopy

Sm(III) exhibits an orange emission, which is normally much weaker than Eu(III) and Tb(III) emission due to the small energy gap ΔE, thus making multiphonon relaxation that much easier.

Monocrystal absorption spectra of SmPhβ$_3$·Phen at 293 and 4.2 K are shown in Fig. 10 and the results of the intensity analysis are collected in Table 3. In the same table the Judd–Ofelt parameters τ_λ are included. Based on the intensities of the respective f-f transitions, the radiative decay rate can be evaluated. Absorption from the $^6H_{5/2}$ ground state to excited states clearly shows lower intensities of the observed transitions, compared to those recorded for Sm(Cl$_3$CCOO)$_3$·2H$_2$O carboxylate,[26] and enhancement of the intensities with decreasing temperature. The above effects suggest a somewhat higher symmetry (though still low) of Sm(III) in the presented system (in comparison to that for the above-mentioned samarium

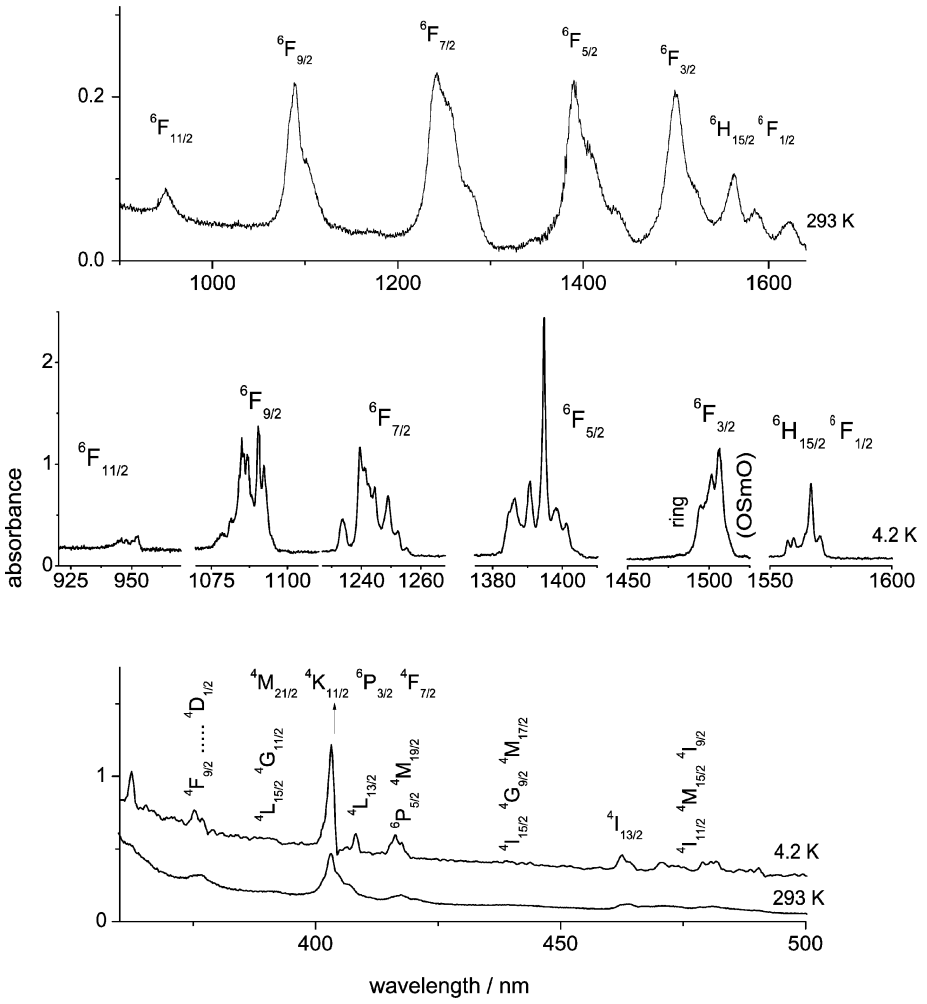

Fig. 10 Absorption spectra of the SmPhβ_3·1,10-Phen crystal at 293 and 4.2 K; assignment of the f-f transitions and vibronic components.

trichloroacetate crystal) and a structural transformation at low temperatures. Although at room temperature the first excited state $^6H_{7/2}$ can be thermally populated, its population is relatively low (~1.8% if a reasonable splitting of 817 cm^{-1} between $^6H_{5/2}$ and $^6H_{7/2}$ is assumed). Thus, the observed increase of intensities with decrease of temperature should be minor. However, the significant increase of oscillator strengths that was observed suggests instead a phase transformation.

The Judd–Ofelt parameters were evaluated with good accuracy and they reproduce well the intensities of the absorption bands observed in the spectrum.

A decrease of temperature leads to separation of the absorption transitions of the samarium ion, especially in the IR spectral region. Finally, in the samarium spectra a doublet structure of the lines was also observed, pointing to two metal sites in the structure. It was difficult to differentiate, at 4.2 K, the two components of the $^6F_{1/2}$ level from those of the $^6H_{15/2}$ one, but splitting of both these levels is smaller than that observed in Sm(III) co-doped in a LaF_3 crystal.[16] The number of lines observed in the 1550–1600 nm range is too small. One would expect 8 for $^6H_{15/2}$ and one for $^6F_{1/2}$ for low-symmetry centre (as the X-ray data suggest, as well as suggested by the results of emission spectral analysis of Eu(III) ions). In contrast, for other transitions, the numbers of lines correspond quite well to the expected values for two metal centres. Most probably some weak components of the $^6H_{15/2}$ transition extend into the range of $^6F_{3/2}$ transitions. Similar results were reported earlier for polynuclear and heteronuclear samarium trichloroacetates.[26]

Table 3 The oscillator strength P of the f-f transitions and the τ_λ values for the SmPhβ_3·1,10-Phen crystal (C_{Sm} = 1.68 mol dm^{-3})

		P·10^{-8}	
$^6H_{5/2}$→	λ/nm	293 K	4.2 K
$^6F_{1/2}$, $^6H_{15/2}$	1640–1541	48.99	53.86
$^6F_{3/2}$	1541–1458	148.08	277.94
$^6F_{5/2}$	1458–1316	203.75	233.87
$^6F_{7/2}$	1316–1163	236.07	239.69
$^6F_{9/2}$	1163–1012	189.76	303.16
$^6F_{11/2}$	1012–914	37.48	53.70
$^4I_{9/2}$, $^4M_{15/2}$, $^4I_{11/2}$	493– 464	117.21	141.85
$^4I_{13/2}$	464–458	33.61	56.06
$^4M_{17/2}$, $^4G_{9/2}$, $^4I_{15/2}$	458–428	41.47	49.71
$^4M_{19/2}$, $^6P_{5/2}$	428–413	59.28	76.01
$^4L_{13/2}$	413–406	75.12	46.42
$^4F_{7/2}$, $^6P_{3/2}$, $^4K_{11/2}$, $^4M_{21/2}$	406–396	284.96	291.31
$^4L_{15/2}$, $^4G_{11/2}$	396–382	34.62	96.34
$^4D_{1/2}$, $^6P_{7/2}$, $^4L_{17/2}$, $^4K_{13/2}$, $^4F_{9/2}$	382–369	83.38	160.71
τ_2·10^{-9}		3.67 ± 1.36	
τ_4·10^{-9}		4.33 ± 0.45	
τ_6·10^{-9}		3.06 ± 0.42	

Silica gels co-doped by Eu(III) chelate

In rigid systems an enhancement of emission can be expected and consequently lanthanide chelates incorporated in silica gels are promising optical materials.[27–31] The silica gels co-doped by Eu(III) chelate were obtained by the sol-gel technique

and the spectroscopic properties of single crystals and gels were compared. The fluorescence spectra obtained at 77 K for EuPhβ$_3$·Phen doped silica sol-gel are presented in Fig. 2. The sol sample was prepared from an acetonitrile solution. The splitting pattern of the Stark components in the fluorescence spectra of EuPhβ$_3$·Phen in silica gel indicates that the environment of Eu^{3+} ion in gel differs from that in the europium crystal. This is most probably due to the replacement of Phen molecules by silica groups in the first coordination sphere of Eu^{3+} ion.[27] This causes, for example, a change in the character of the Ln–ligand bonding that could affect the intensity of f-f transitions in the lanthanide ions doped in sol samples, and finally could lead to different fluorescence properties of the sol-gel system under study. To check the process of exchange of phenanthroline molecules in the chelate incorporated in the gel selective excitation of emission was used. No energy transfer was observed using the 350 nm line and a stronger emission was detected using direct excitation of the $^5L_6$ level. Further studies of the gel systems, including with Sm(III) chelates, will be the subject of future reports.

Conclusions

Lanthanide mixed chelates of the type LnPhβ$_3$·Phen [where: Ln = Sm, Eu, Tb; Phβ = CCl_3–C(O)–N–P(O)–$(OCH_3)_2$; Phen = 1,10-phenanthroline] form an isostructural series. The X-ray diffraction studies detected two different structural sites for Sm^{3+} ions in the SmPhβ$_3$·Phen monocrystal.

Analysis of the absorption spectra at 293 K for LnPhβ$_3$·Phen (Ln = Sm, Eu) crystals shows that the intensities of the 4f-4f transitions are slightly lower in comparison to those in $Sm(Cl_3CCOO)_3·2H_2O$ single crystal,[26] which confirms the somewhat higher (but still low) symmetry of Ln(III) sites in the structure presented here. The Sm(III) spectra are more complex than that expected for a one-site symmetry of Sm(III), in agreement with X-ray results.

Efficient energy transfer sensitises the interion emission from $^5D_4$ or $^5D_0$ levels of Tb(III) and Eu(III) after ligand band excitation; an energy level diagram was proposed and the mechanism of energy transfer (E-T) discussed.

Two different structural sites for the Ln^{3+} ions are seen in the fluorescence spectra of EuPhβ$_3$·Phen crystal at 77 K. This was perfectly observed in the doublet splitting of the $^5D_0 \rightarrow {}^7F_0$ transition, as well as in the doublet structure of both the $^5D_0 \rightarrow {}^7F_1$ and $^5D_0 \rightarrow {}^7F_2$ bands.

Vibronic components in the $^7F_0 \rightarrow {}^5D_2$ transition of the Eu^{3+} ion in the fluorescence excitation spectra at 77 K were analysed and strong vibronic coupling with ligand internal vibrations was observed. Based on the comparison of the IR and emission spectra, a resonance effect was discovered and δ(OPO) or ν(OLnO)*$\pi(\varphi)$; $\delta(CCl_3)$*$\delta(\phi_n)$ modes were determined to be responsible for this phenomenon.

Acknowledgements

The authors would like to thank K. V. Domasevitch for help in performing the X-ray measurements. The authors acknowledge partial financial support from the Polish Committee for Scientific Research (grant no. 3TO9A04018).

References

1 E. Aminaka, T. Tsutsui and Sh. Saito, *Jpn. J. Appl. Phys.*, 1994, **33**, 1061.
2 V. Tsaryuk, J. Legendziewicz, V. Zolin, L. Puntus and J. Sokolnicki, in *Proceedings of 9th Cimtec-World Forum on New Materials: Advances in Science and Technology, 27*, eds. P. Vicenzini and G.C. Righini, Techna Srl Faenza, Italy, 1999, p. 299.
3 V. Tsaryuk, V. Zolin and J. Legendziewicz, *Spectrochim. Acta A*, 1998, **54**, 2247.
4 J. Legendziewicz, *J. Alloys Compd.*, 2000, **300–301**, 71.
5 O. N. Riebrova, W. N. Biyushkin, T. I. Malinowski, L. D. Procenko and T. I. Dnieprova, *Dokl. Akad. Nauk USSR*, 1982, **266**, 1391.
6 P. G. Sammes and G. Yahioglu, *Chem. Soc. Rev,*, 1994, 327.
7 J.-C. G. Bünzli, E. Moret, V. Foiret, K. J. Schenk, W. Mingzhao and J. Linpei, *J. Alloys Compd.*, 1994, **207/208**, 107.
8 V. Amirkhanov, C. Jańczak, L. Macalik, J. Hanuza and J. Legendziewicz, *J. Appl. Spectrosc.*, 1995, **62**, 5.
9 J. Sokolnicki, J. Legendziewicz, V. Amirkhanov, V. Ovchinnikov, L. Macalik and J. Hanuza, *Spectrochim. Acta A*, 1999, **55**, 349.
10 A. W. Kirsanov and G. I. Derkatch, *Zh. Org. Khim.*, 1956, **26**, 2631.
11 V. Amirkhanov, V. Trush, A. Kapszuk and V. Skopenko, *Zh. Neorg. Khim.*, 1996, **41**, 2052.
12 J. Legendziewicz, K. Bukietyńska and G. Oczko, *J. Inorg. Nucl. Chem.*, 1981, **43**, 2393; J. Legendziewicz, *Wiadomości Chemiczne*, 1988, **42**, 605.
13 R. B. Judd, *Phys. Rev.*, 1962, **127**, 750.
14 G. S. Ofelt, *J. Chem. Phys.*, 1962, **37**, 511.
15 W. T. Carnall, P. R. Fields and K. Rajnak, Argonne Natl. Lab. Rep., ANL 7358, 1967, Electronic Energy Levels in Trivalent Lanthanide Aquo Ions.
16 W. T. Carnall, P. R. Fields and K. Rajnak, *J. Chem. Phys.*, 1967, **49**, 4412; W. T. Carnall, P. R. Fields and K. Rajnak, *J. Chem. Phys.*, 1967, **49**, 4424; W. T. Carnall, P. R. Fields and K. Rajnak, *J. Chem. Phys.*, 1967, **49**, 4443; W. T. Carnall, P. R. Fields and K. Rajnak, *J. Chem. Phys.*, 1967, **49**, 4447; W. T. Carnall, P. R. Fields and K. Rajnak, *J. Chem. Phys.*, 1967, **49**, 4450.
17 G. M. Sheldrick,SHELXS-86 *Acta Crystallogr., Sect. A*, 1990, **46**, 467.
18 G. M. Sheldrick, SHELXL-93, A System of Computer Programs for X-ray Structure Determination, University of Göttingen, Göttingen, Germany, 1993.
19 L. Thompson, J. Legendziewicz, J. Cybińska, Li Pan and W. Brennessel, *J. Alloys Compd.*, 2002, **341**, 312.
20 M. Borzechowska, V. Trush, I. Turowska-Tyrk, W. Amirkhanov and J. Legendziewicz, *J. Alloys Compd.*, 2002, **341**, 98.
21 R. D. Peacock, *Structure Bond.*, 1975, **22**, 83.
22 J. Legendziewicz, *J. Alloys Compd.*, 2002, **341**, 34.
23 G. Blasse, G. J. Dirksen, N. Sabbatini, S. Perathoner, J. M. Lehn and B. Alpha, *J. Phys. Chem.*, 1988, **92**, 2419.
24 A. Dossing, J. Sokolnicki, J. P. Riehl and J. Legendziewicz, *J. Alloys Compd.*, 2002, **341**, 150.
25 J. Legendziewicz, G. Oczko, V. Amirkhanov, R. Wiglusz and V. A. Ovchynnikov, *J. Alloys Compd.*, 2000, **300/301**, 360 and citations therein.
26 J. Legendziewicz, M. Borzechowska, G. Oczko and G. Meyer, *New J. Chem.*, 2000, **24**, 53.
27 J. Sokolnicki, K. Maruszewski, W. Stręk and J. Legendziewicz, *J. Sol-Gel Sci. Technol.*, 1998, **13**, 611.
28 K. Driesen, P. Lenaerts, K. Binnemans and C. Görller-Walrand, *Phys. Chem. Chem. Phys.*, 2002, **4**, 552.
29 H. F. Brito, O. L. Malta and J. F. S. Menezes, *J. Alloys Compd.*, 2000, **303/304**, 336.
30 J. Legendziewicz, W. Strêk, J. Sokolnicki, D. Hreniak and V. Zolin, *Opt. Mater.*, 2002, **19**, 175.
31 J. Sokolnicki, J. Legendziewicz and J. P. Riehl, *J. Phys. Chem. B*, 2002, **106**, 1508.